Supporting Information

Elucidating the Cooperative Roles of Water and Lewis Acid–Base Pairs in Cascade C–C Coupling and Self-Deoxygenation Reactions

Houqian Li, [‡] Dezhou Guo,[†,‡] Nisa Ulumuddin,[†,‡] Nicholas R. Jaegers,[‡,§] Junming Sun,[*,‡] Bo Peng,[§] Jean-Sabin McEwen,[‡,§,⊥,∥,#] Jianzhi Hu,[§,‡] Yong Wang,[*,‡,§]

‡The Gene & Linda Voiland School of Chemical Engineering and Bioengineering, Washington State University, Pullman, Washington 99164, United States

§Institute for Integrated Catalysis, Pacific Northwest National Laboratory, Richland, Washington 99352, United States

⊥Department of Physics and Astronomy, Washington State University, Pullman, Washington 99164, United States

∥Department of Chemistry, Washington State University, Pullman, Washington 99164, United States

#Department of Biological Systems Engineering, Washington State University, Pullman, Washington 99164, United States

*Email: junming.sun@wsu.edu.

*Email: yong.wang@pnnl.gov.

† D. Guo and N. Ulumuddin contributed equally to this work.

Section S1.

Figure S1: Top view of the possible configurations of the dehydrated $Zn_1Zr_{11}O_{12}$ surface in which a Zr^{4+} is substituted by a Zn^{2+}, and two protons are systematically tested for charge compensation based on the surface morphology.

Figure S2: (A) Relative energy comparisons of possible conformations that were tested when replacing a Zr^{4+} to a Zn^{2+} and charge compensating it with two nearby protons in the first layer of the surface; (B) Top view of the most favorable $Zn_1Zr_{11}O_{12}$ surface.

Figure S3: Top view of the possible configurations of a hydrated $Zn_1Zr_{11}O_{12}$ surface.

Figure S4: (A) Relative adsorption energies for the dissociative adsorption of water into a OH and a H adspecies on a $Zn_1Zr_{11}O_{12}$ surface; (B, C) Top view of the two most favorable configurations on a hydrated $Zn_1Zr_{11}O_{12}$ surface.

Figure S5: DRIFTS-OH (A) and XRD (B) of fresh and spent (24 h time on stream, P_{H_2O}/P_{Ace}=10.7 kPa/1 kPa, space velocity=0.03 $mol_{Ace}/g_{cat}/h$) $Zn_1Zr_{10}O_z$.

Figure S6: DRIFTS of Acetone adsorption at 298 K and desorption at 723 K (A) followed by water flowing at 723 K using a sample surface before introducing water as background (B).

Figure S7: Conversion and selectivities as a function of time-on-stream over $Zn_1Zr_{10}O_z$ (723 K, $P_{Ace}/P_{H_2O} = 1.4\ kPa/3.2\ kPa$, balance N_2).

Figure S8: Acetone conversion and isobutene selectivity as a function of inverse flow rate during steady-state ATIB reaction on $Zn_1Zr_{10}O_z$ at 723 K.

Figure S9: ATIB reaction stability over $Zn_1Zr_{10}O_z$ at different conditions.

Figure S10: Catalyst evaluation of fresh sample and 10-time-regenerated sample.

Figure S11: comparison of acetone to isobutene reaction and acetic acid ketonization on $Zn_1Zr_{10}O_z$.

Figure S12. Measured TOF_{IB} under P_{Ace}=0.7 kPa, P_{H_2O}=0 kPa (A) and P_{Ace}=0.7 kPa, P_{H_2O}=0.4 kPa (B).

Figure S13. Selectivity and conversion as a function of time on stream under P_{Ace}=0.7 kPa, 723 K (A) and P_{Ace}=0.7 kPa, P_{H_2O}=0.4 kPa, 723 K (B).

Figure S14: Distinct position and corresponding number of each site for DAA adsorption site on the Dehydrated Surface (A) and Hydrated Surface (B) models.

Figure S15: Top view for the horizontal configuration of DAA adsorbed at plausible positions with FGs pointing perpendicularly away from the surface (FG upside) on a dehydrated $Zn_1Z_{11}O_{12}$ surface.

Figure S16: Top view for the vertical configuration of DAA adsorbed at plausible positions with FGs pointing perpendicularly away from the surface (FG upside) on a dehydrated $Zn_1Z_{11}O_{12}$ surface.

Figure S17: Top view for the horizontal configuration of DAA adsorbed at plausible positions with FGs pointing toward the surface (FG downside) on a dehydrated $Zn_1Z_{11}O_{12}$ surface.

Figure S18: Top view for the vertical configuration of DAA adsorbed at plausible positions with FGs pointing toward the surface (FG downside) on a dehydrated $Zn_1Z_{11}O_{12}$ surface.

Figure S19: (A) The adsorption energies of possible adsorption sites for the DAA molecule with its FGs pointing away from a dehydrated $Zn_1Z_{11}O_{12}$ $(\bar{1}11)$ surface. (B) Top and side view for the adsorption of DAA at site 10 as marked by the red circle in panel A on a dehydrated $Zn_1Z_{11}O_{12}$ surface.

Figure S20: Top view for the horizontal configuration of DAA adsorbed at plausible positions on the Hydrated Surface 1.

Figure S21: Top view for the vertical configuration of DAA adsorbed at plausible positions on the Hydrated Surface 1.

Figure S22: Top view for the horizontal configuration of DAA adsorbed at plausible positions on the Hydrated Surface 2.

Figure S23: Top view for the vertical configuration of DAA adsorbed at plausible positions on the Hydrated Surface 2.

Figure S24: (A, C) Top and side view of DAA at the sites within the vicinity of the adsorbed H on Hydrated Surface 2; (B, D) at the corresponding sites on the dehydrated $Zn_1Z_{11}O_{12}$ surface.

Table S1: Adsorption energy, distortion energy and number of transferred electrons for systems in Figure S23.

Section S2.

Derivation of the rate equation for the acetone-DAA-isobutene kinetic model.

S1.

The clean $Zn_xZr_yO_z$ surface was modeled by replacing a Zr^{4+} to a Zn^{2+} in the first layer the surface, forming a $Zn_1Zr_{11}O_{12}$ stoichiometric catalyst. However, the charge difference needs to be compensated. As such, several ways have been tried to balance the charges and found that balancing the surface with two adsorbed protons provides the most stable environment for both Zn^{2+} and diacetone alcohol (DAA) molecule. Then, we configurationally scanned plausible positions for two protons based on the surface morphology (as shown in **Figure S1**) and obtained the most favorable conformation (based on the underlying energetics as shown in **Figure S2A**) shown in **Figure S2B**.

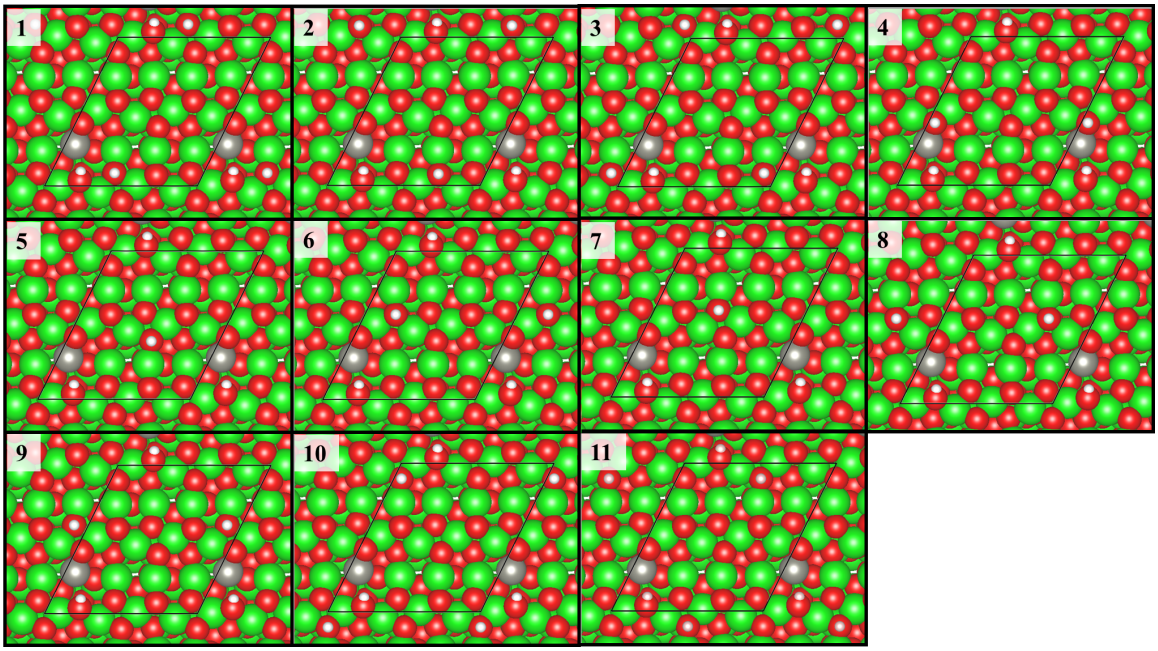

Figure S1. Top view of the possible configurations of dehydrated $Zn_1Zr_{11}O_{12}$ surface. A Zr^{4+} is substituted by a Zn^{2+}, and two protons are systematically tested for charge compensation based on the surface morphology. The Zr, Zn, O and H atoms or ions are represented by green, gray, red, and white spheres, respectively.

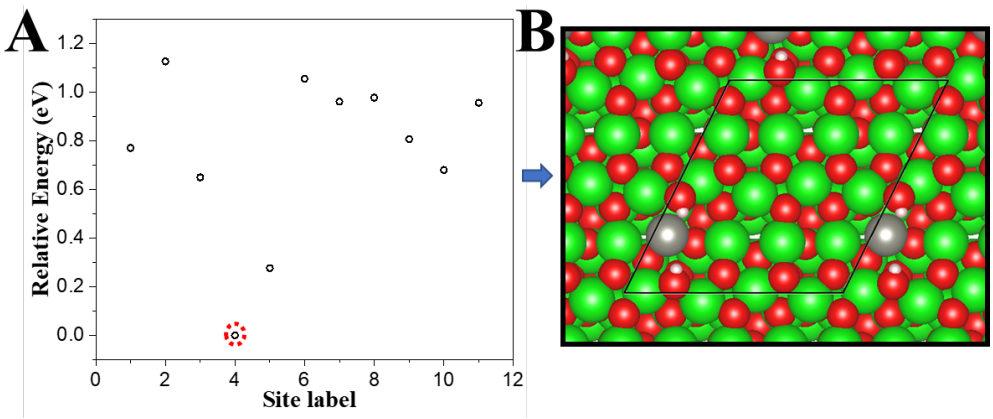

Figure S2. (A) Relative energies comparison of possible conformations that were tested when replacing a Zr^{4+} to a Zn^{2+} and charge compensating it with two nearby protons in the first layer of the surface. (B) Top view of the most favorable $Zn_1Zr_{11}O_{12}$ surface, which is indicated by the dashed red circle in panel A. The Zr, Zn, O and H atoms or ions are represented by green, gray, red, and white spheres, respectively.

The hydrated surface has been model by adding a water molecule on the dehydrated surface. As suggested by the previous DFT results, water molecules very easily dissociate on a m-ZrO_2 $(\bar{1}11)$ surface with a low activation barrier of 5.6 kJ/mol[1]. Consequently, we have systematically tested the possible positions for OH and H adspecies on the surface, as shown in Figure S3. Considering the complexity of the of the adsorption of on a m-ZrO_2 $(\bar{1}11)$ surface, two candidates are considered herein as shown in Figure S4B and S4C since they were the two most favorable configurations as indicated in Figure S4A. These two configurations were labeled as the Hydrated Surface Type 1 and Hydrated Surface Type 2.

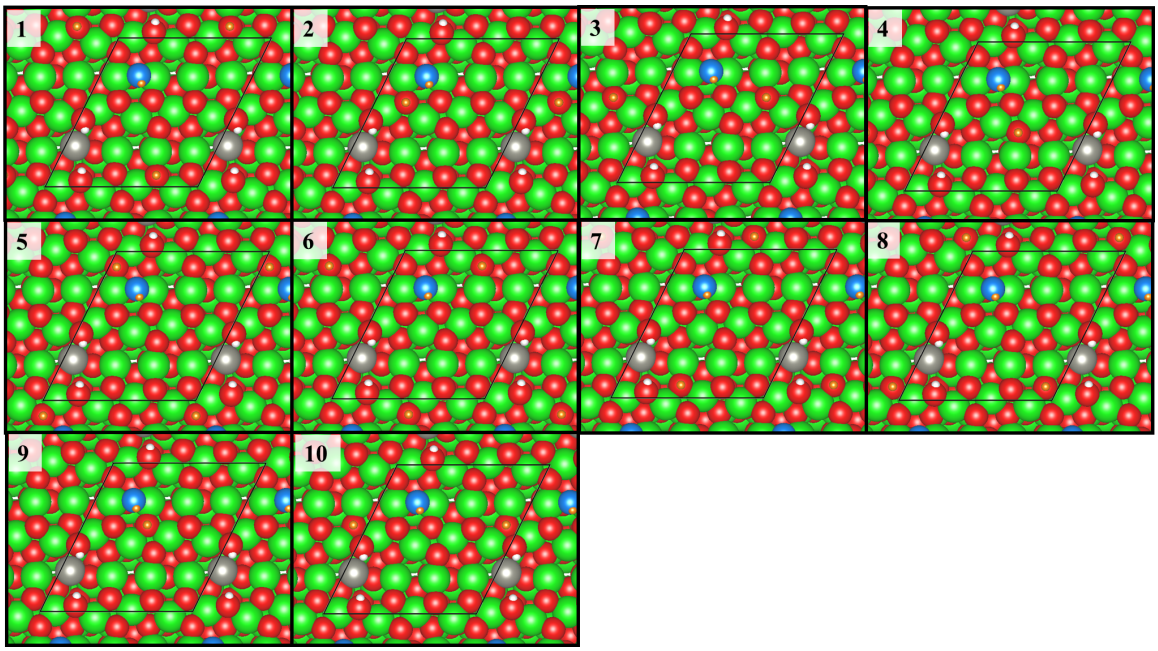

Figure S3. Top view of the possible configurations of hydrated $Zn_1Zr_{11}O_{12}$ surface. The Zr, Zn, O and H atoms or ions are represented by green, gray, red, and white spheres, respectively. The adsorbed O and H atoms resulting from the dissociative adsorption of water are represented by blue and orange spheres, respectively, for clarity.

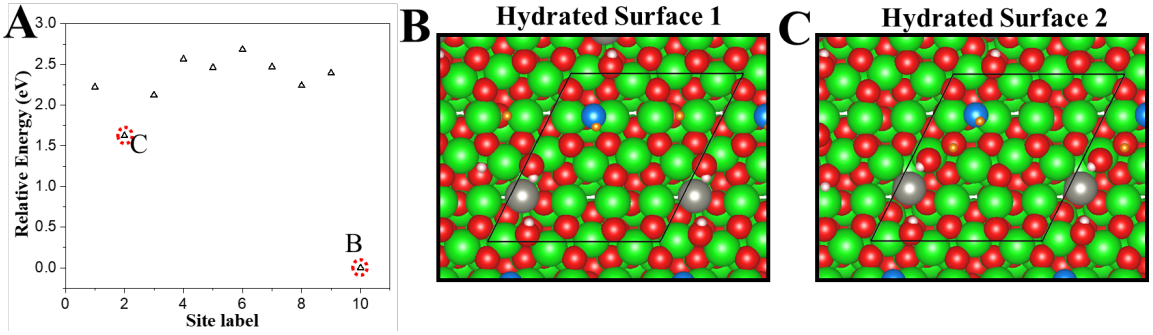

Figure S4. (A) Relative adsorption energies for the dissociative adsorption of water into a OH and a H adspecies on a $Zn_1Zr_{11}O_{12}$ surface. (B, C) Top view of the two most favorable configurations on a hydrated $Zn_1Zr_{11}O_{12}$ surface as indicated with a dashed red circle in A. The Zr, Zn, O and H atoms or ions are represented by green, gray, red, and white spheres, respectively. The adsorbed O and H atoms are represented by blue and orange spheres, respectively, for clarity.

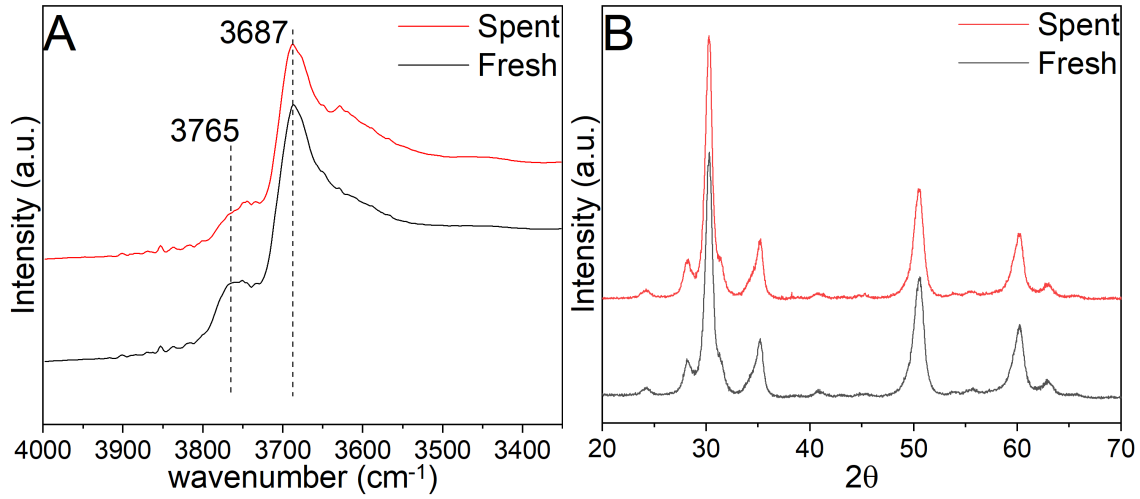

Figure S5: DRIFTS-OH (A) and XRD (B) of fresh and spent (24 h time on stream, P_{H_2O}/P_{Ace}=10.7 kPa/1 kPa, space velocity=0.03 $mol_{Ace}/g_{cat}/h$) $Zn_1Zr_{10}O_z$.

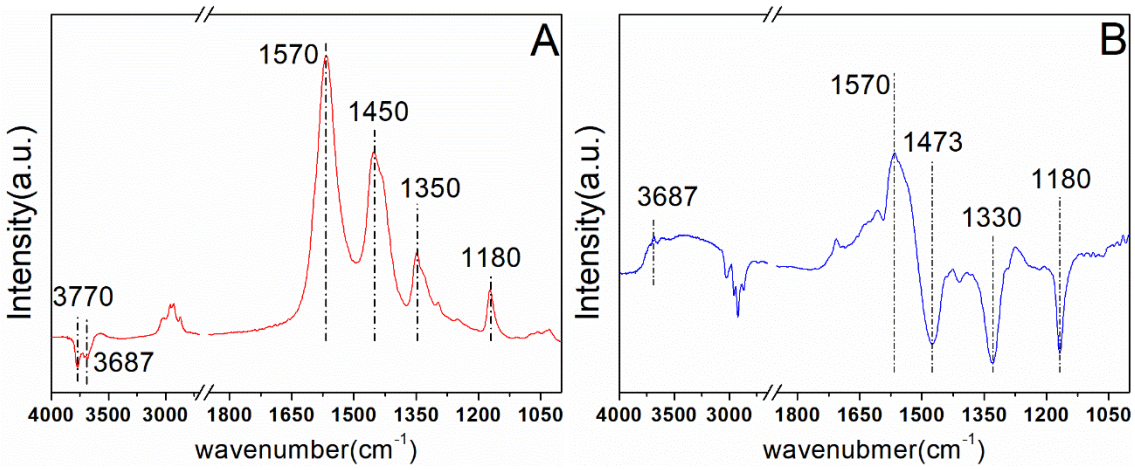

Figure S6. DRIFTS of Acetone adsorption at 298 K and desorption at 723 K (A) followed by water flowing at 723 K using a sample surface before introducing water in the background (B).

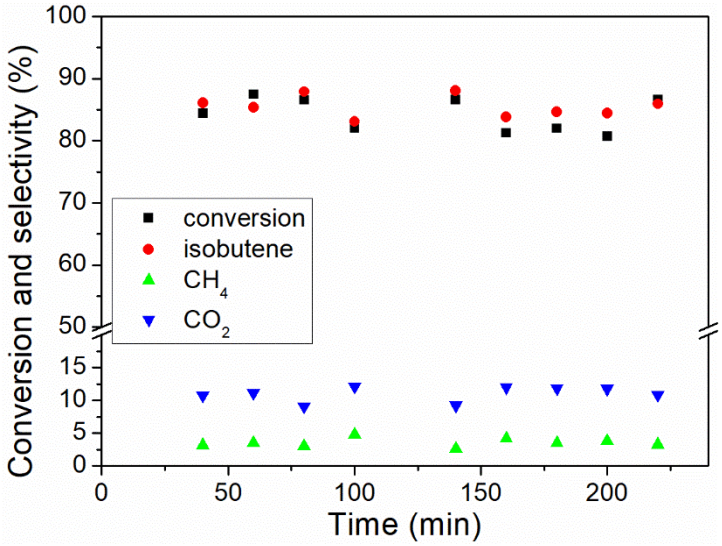

Figure S7. Conversion and selectivities as a function of time-on-stream over $Zn_1Zr_{10}O_z$ (723 K, $P_{Ace}/P_{H_2O} = 1.4\ kPa/3.2\ kPa$, balance N_2).

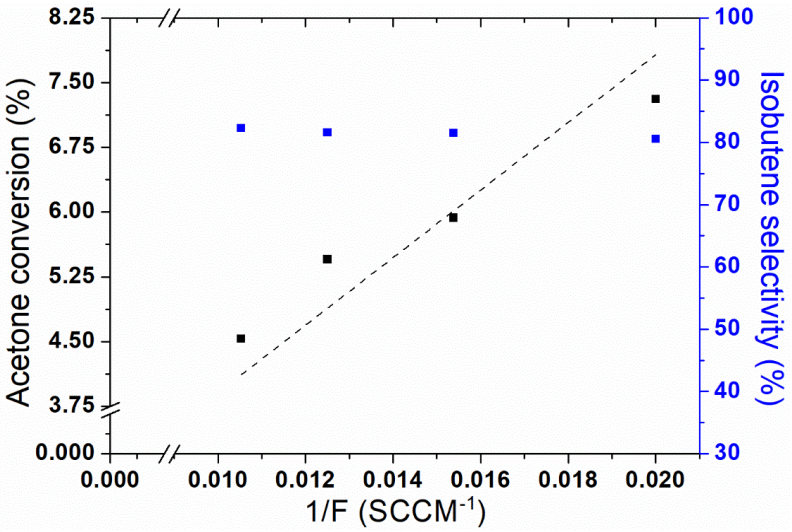

Figure S8. Acetone conversion and isobutene selectivity as a function of inverse flow rate during steady-state acetone-to-isobutene (ATIB) reaction on $Zn_1Zr_{10}O_z$ at 723 K.

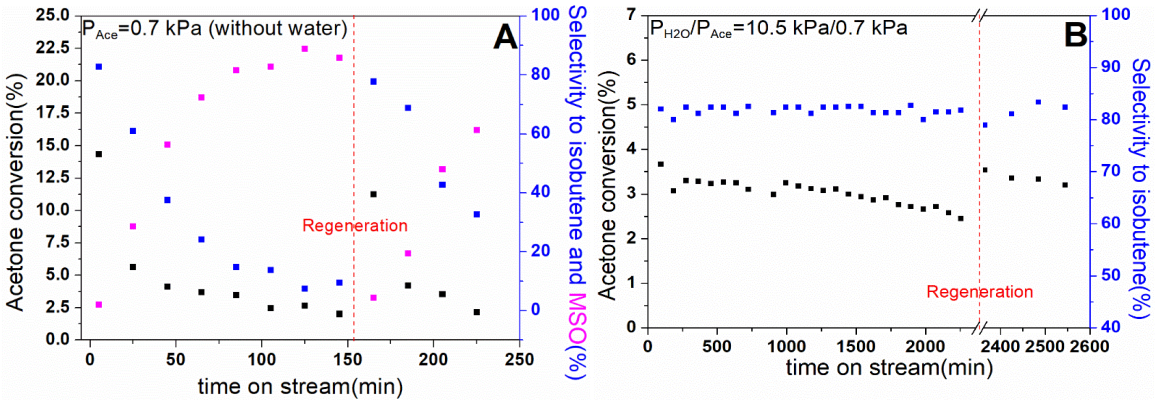

Figure S9. ATIB reaction stability over $Zn_1Zr_{10}O_z$ at different conditions, T=723 K, Space Velocity = 0.243 $mol_{Ace}/g_{cat}/h$ (A), 0.312 $mol_{Ace}/g_{cat}/h$ (B).

In **Figure S9A**, the isobutene formation rate decays exponentially (e.g., $r(t)=r_0 \cdot \exp(-k_d \cdot t)$), which is commonly observed in acetone surface reactions[2-3]. Concomitant occurrence of decreasing isobutene selectivity (blue) and increasing mesityl oxide (MSO) selectivity (magenta) suggest that the transition state of MSO formation scavenges that of isobutene formation in the absence of cofed water which was also observed in **Figure 4**.

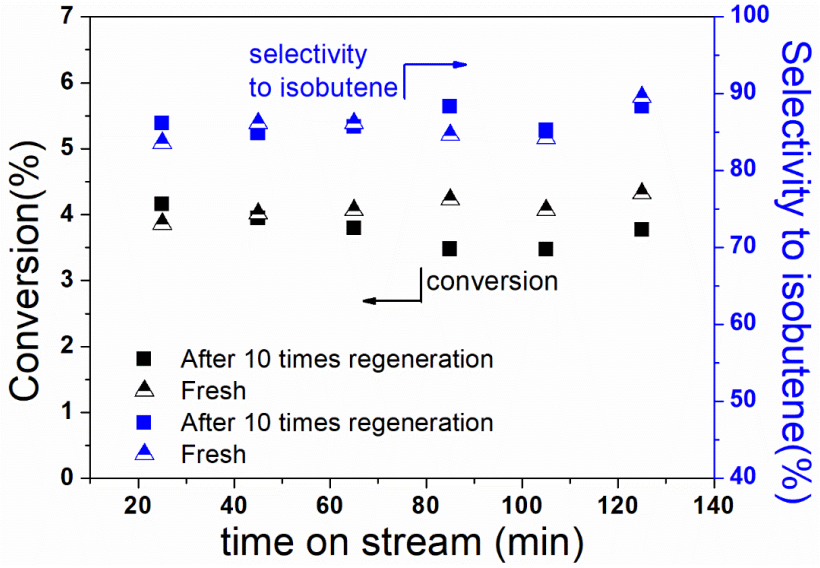

Figure S10. Acetone conversion and selectivity to isobutene on $Zn_1Zr_{10}O_z$ as a function of time-on-stream for fresh a catalyst and 10-time-regenerated catalyst (723 K, P_{H_2O}/P_{Ace}=5.3 kPa/0.5 kPa, space velocity = 0.25 $mol_{Ace}/g_{cat}/h$).

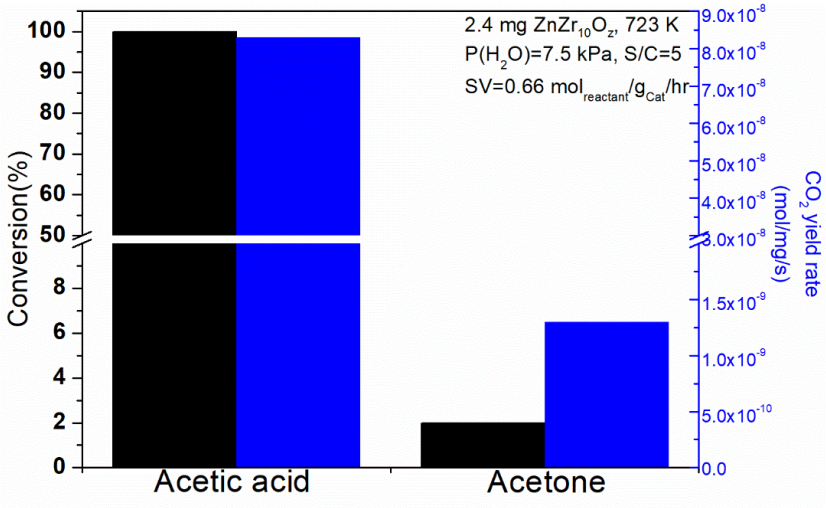

Figure S11. Comparison of acetone to isobutene reaction and acetic acid ketonization on $Zn_1Zr_{10}O_z$.

To examine acetate ketonization on $Zn_xZr_yO_z$, an acetic acid solution was used as the reactant and tested as exhibited in **Figure S11**. CO_2 is produced via acetate ketonization with both acetone and acetic acid acting as the reactant. Therefore, the CO_2 yield rate should be comparable in these two scenarios if acetate ketonization is the rate limiting step in ATIB. However, under the same water pressure and steam to carbon ratio, conversion and CO_2 yield rate for acetic acid ketonization are much greater than that for the ATIB reaction. Even at a lower temperature and larger space velocity, much higher CO_2 yield rate was observed in acetic ketonization instead of in ATIB. These imply that adsorbed acetate undergoes rapid ketonization which results in water, acetone, and CO_2.

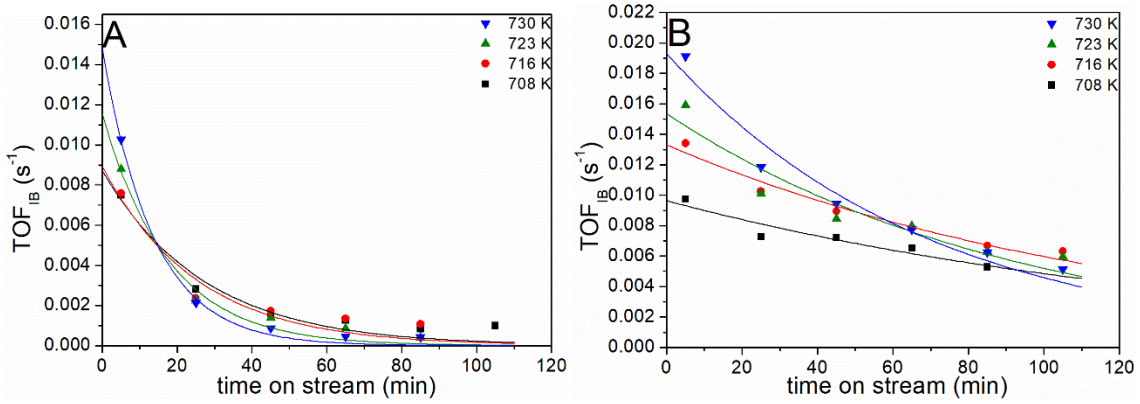

Figure S12. Measured TOF_{IB} (conversion<7%) under P_{Ace}=0.7 kPa, P_{H_2O}=0 kPa (A) and P_{Ace}=0.7 kPa, P_{H_2O}=0.4 kPa (B). Solid lines represent regressed fits of the data to the form of $\boldsymbol{r(t) = r(0) \cdot \exp(-k_d t)}$.

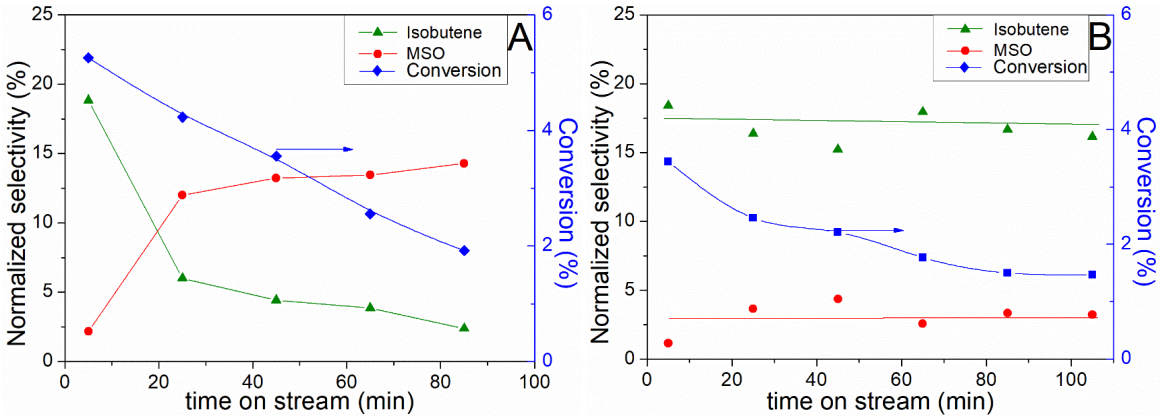

Figure S13. Selectivity and conversion as a function of time on stream under P_{Ace}=0.7 kPa, 723 K (A) and P_{Ace}=0.7 kPa, P_{H_2O}=0.4 kPa, 723 K (B). Normalized selectivities are the selectivities divided by number of carbons in the product. Solid lines serve to guide the eye.

From the fit of the rate data to Eq (5), acetone adsorption constant is much larger than that of water ($K_{ads,Ace}/K_{ads,H_2O}$>10) at 723 K which is consistent with Rorrer et al. reported at relatively lower temperature[4]. It suggests that water coverage could be ignored compared with the adsorbed acetone, especially at lower water partial pressure employed in this experiment (i.e., P_{H_2O}= 0.4 kPa). Despite of the negligible water coverage, the surface reaction chemistry seems drastically changed, evidenced by drastically decreased selectivity to MSO and thus hampered deactivation in **Figure S12**.

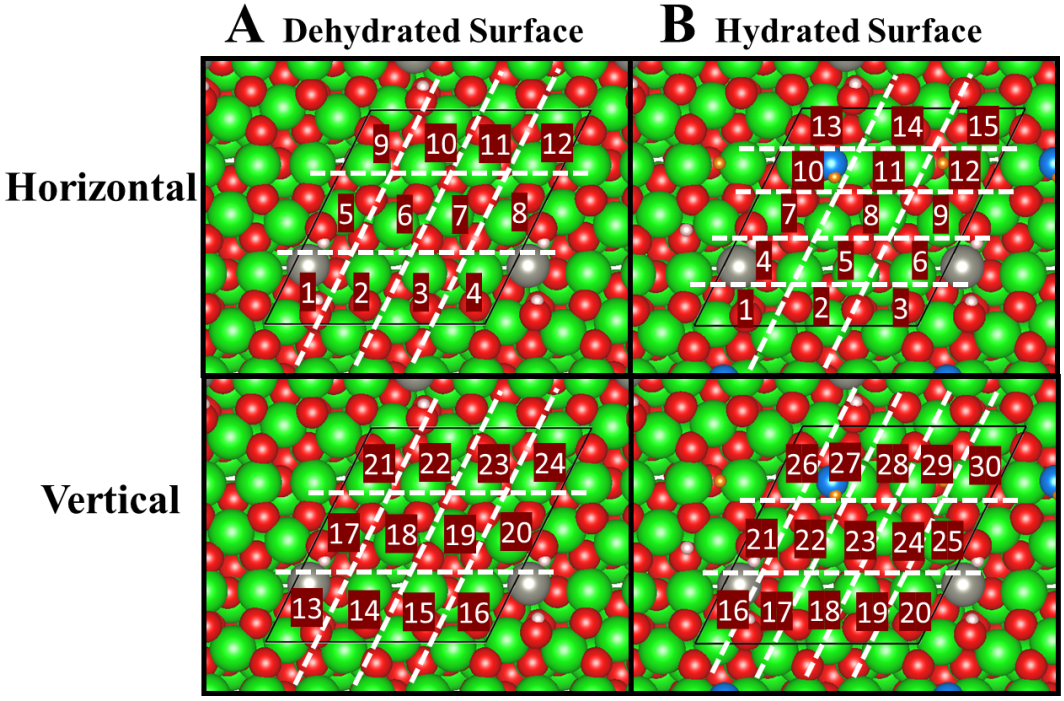

Figure S14. Distinct position and corresponding number of each site for DAA adsorption site on the model Dehydrated Surface (A), Hydrated Surface (B). Both the horizontal and vertical configurations of DAA absorbing on the surfaces are considered. The Zr, Zn, O and H atoms or ions are represented by green, gray, red, and white spheres, respectively. The adsorbed O and H atoms are represented by blue and orange spheres, respectively, for clarity.

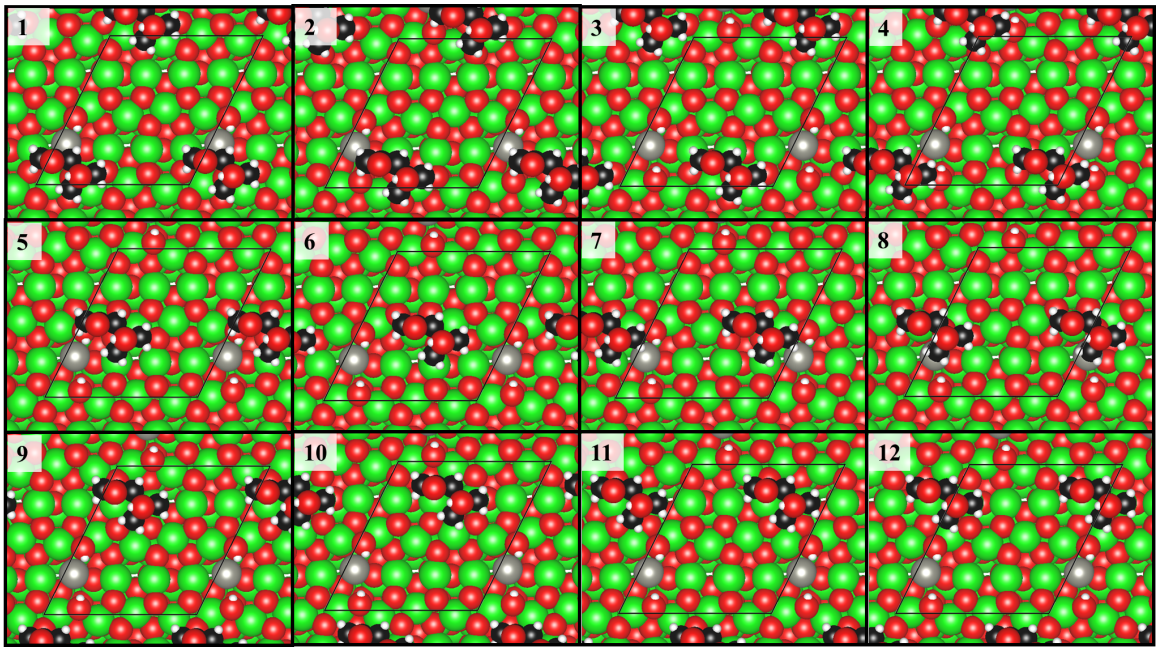

Figure S15. Top view for the horizontal configuration of DAA adsorbed at plausible positions with functional groups point perpendicularly away from the surface (FG upside) on a dehydrated

$Zn_1Z_{11}O_{12}$ surface. The Zr, Zn, C, O and H atoms or ions are represented by green, gray, black, red, and white spheres, respectively.

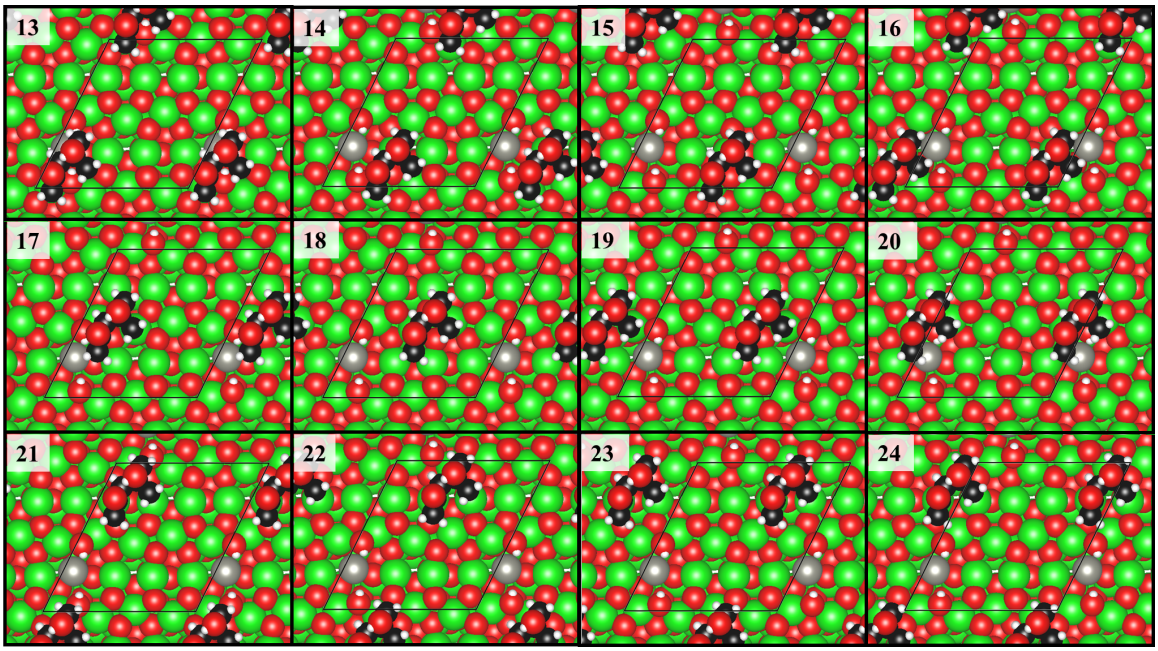

Figure S16. Top view for the vertical configuration of DAA adsorbed at plausible positions with functional groups point perpendicularly away from the surface (FG upside) on a dehydrated $Zn_1Z_{11}O_{12}$ surface. The Zr, Zn, C, O and H atoms or ions are represented by green, gray, black, red, and white spheres, respectively.

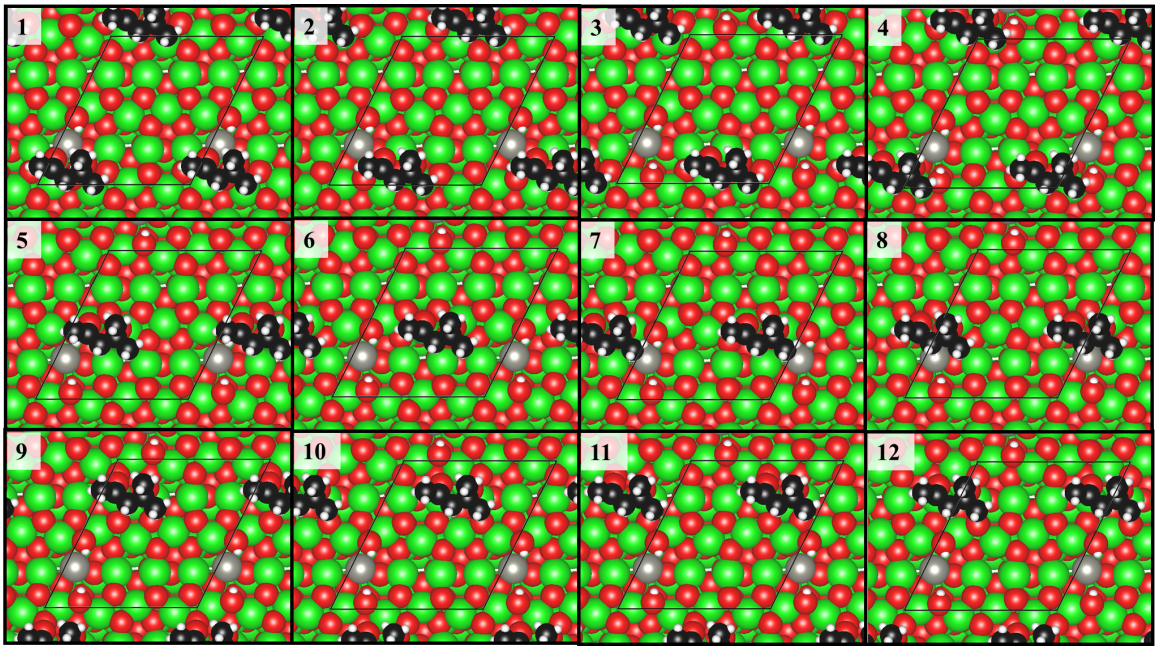

Figure S17. Top view for the horizontal configuration of DAA adsorbed at plausible positions with functional groups point toward the surface (FG downside) on a dehydrated $Zn_1Z_{11}O_{12}$ surface. The Zr, Zn, C, O and H atoms or ions are represented by green, gray, black, red, and white spheres, respectively.

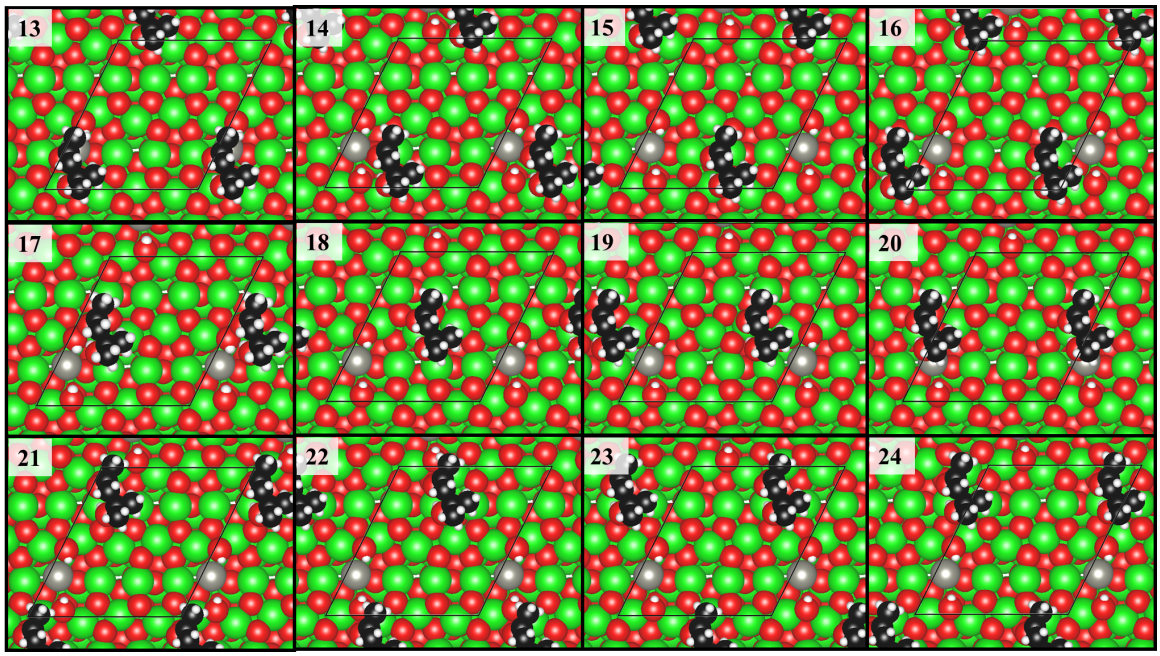

Figure S18. Top view for the vertical configuration of DAA adsorbed at plausible positions with functional groups point toward the surface (FG downside) on a dehydrated $Zn_1Z_{11}O_{12}$ surface. The Zr, Zn, C, O and H atoms or ions are represented by green, gray, black, red, and white spheres, respectively.

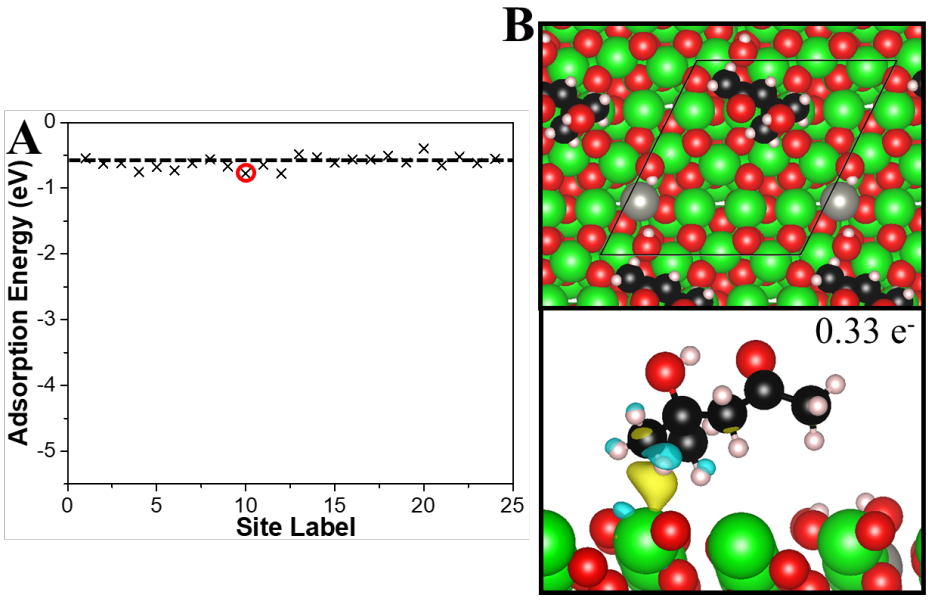

Figure S19. (A) The adsorption energies of possible adsorption sites for the DAA molecule with its functional groups (FG) pointing away from a dehydrated $Zn_1Z_{11}O_{12}$ ($\bar{1}11$) surface. (B) Top and side view for the adsorption of DAA at site 10 as marked by the red circle in panel A on a dehydrated $Zn_1Z_{11}O_{12}$ surface. The Zr, Zn, C, O and H atoms or ions are represented by green, gray, black, red and white spheres, respectively. The areas indicated in yellow represent those of electron gain while those in blue are those of electron loss upon the adsorption of the DAA

molecule at an isosurface level of 0.002 electrons/Bohr^3. The average adsorption energy value is marked by a black dashed line.

To explain how the adsorbed surface proton affects the DAA molecule's adsorption configuration on the $Zn_1Z_{11}O_{12}$ surface, all possible adsorption sites have been tested that are shown in **Figures S14-S24**. In addition to what is discussed in the main text, we also considered when the functional group of DAA adsorbs perpendicularly away from the surface (the cases where DAA's functional groups (FGs) point toward from the surface is considered in the main text). The corresponding site numbers and the top view of configurations are shown in **Figure S14-S16**. The corresponding 24 distinct adsorption energies are plotted in **Figure S19A**. We have found a weak average adsorption energy of -0.61 eV for this configuration. To understand these results better, we took the adsorption configurations at Site 10 as an example and performed a corresponding charge density difference analysis and calculated the mean absolute charge transfer as shown in **Figure S19B**. We found the surface interacts with the adsorbate mainly through weak dipole-dipole interactions with the C and H atoms, indicated by the little charge transfer of 0.33 electrons. The dipole-dipole interaction is also implied by the 2-3 Å bond length between the DAA and the surface. As compared with the strong adsorption energy of -5.31 eV at the corresponding site when the FGs of DAA point toward the surface, it is unlikely for DAA to adsorb on the $Zn_xZ_yO_z$ surface with its FGs pointing away from the surface.

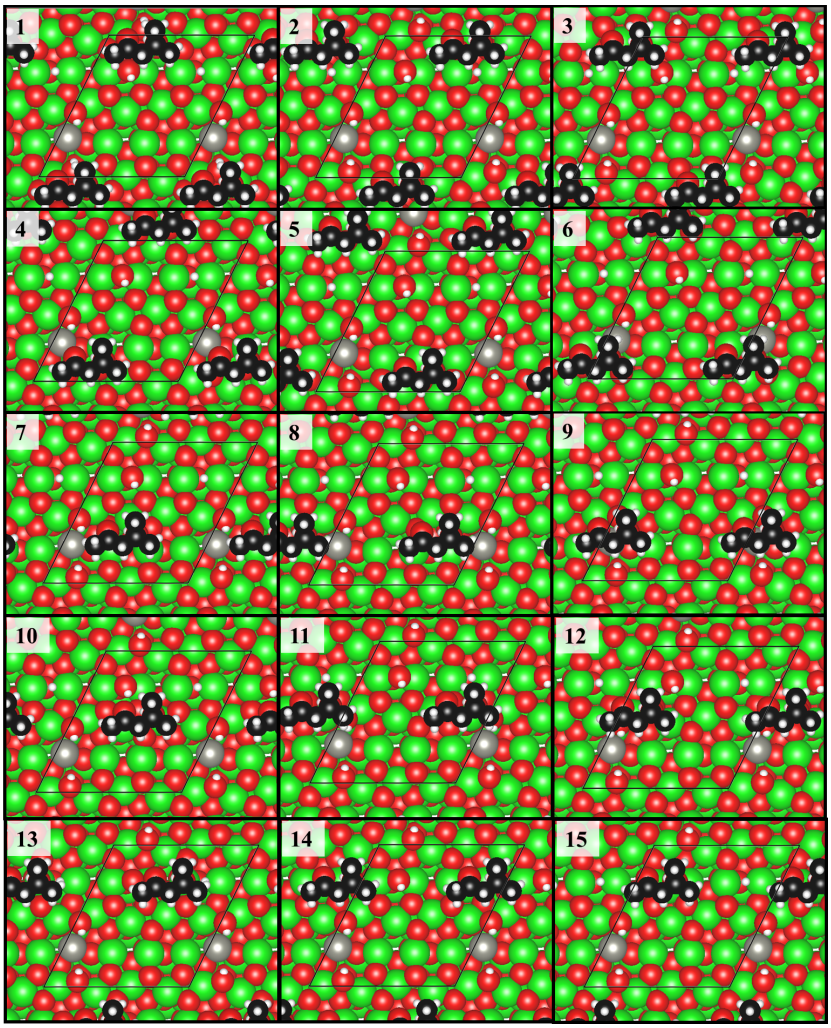

Figure S20. Top view for the horizontal configuration of DAA adsorbed at plausible positions on the Hydrated Surface 1. The Zr, Zn, C, O and H atoms or ions are represented by green, gray, black, red, and white spheres, respectively.

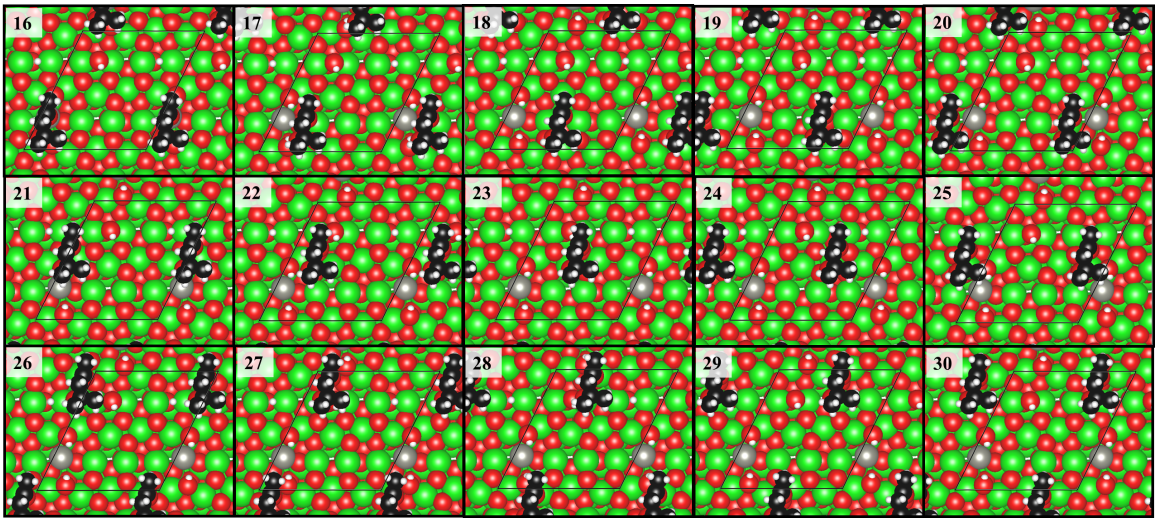

Figure S21. Top view for the vertical configuration of DAA adsorbed at plausible positions on the Hydrated Surface 1. The Zr, Zn, C, O and H atoms or ions are represented by green, gray, black, red, and white spheres, respectively.

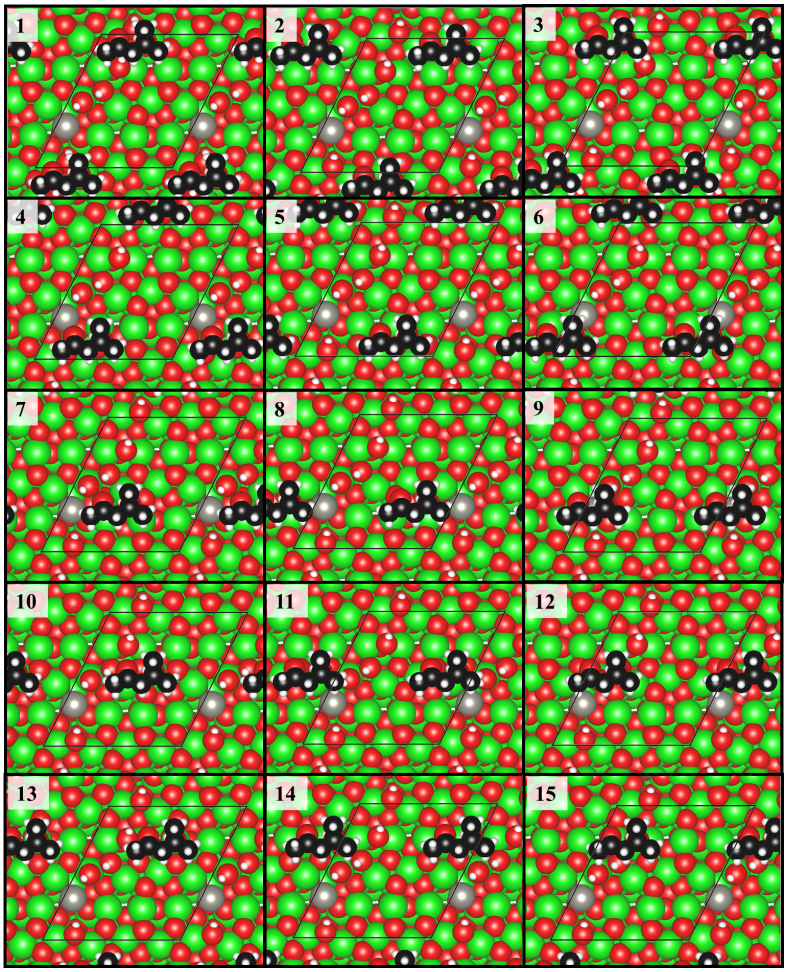

Figure S22. Top view for the horizontal configuration of DAA adsorbed at plausible positions on the Hydrated Surface 2. The Zr, Zn, C, O and H atoms or ions are represented by green, gray, black, red, and white spheres, respectively.

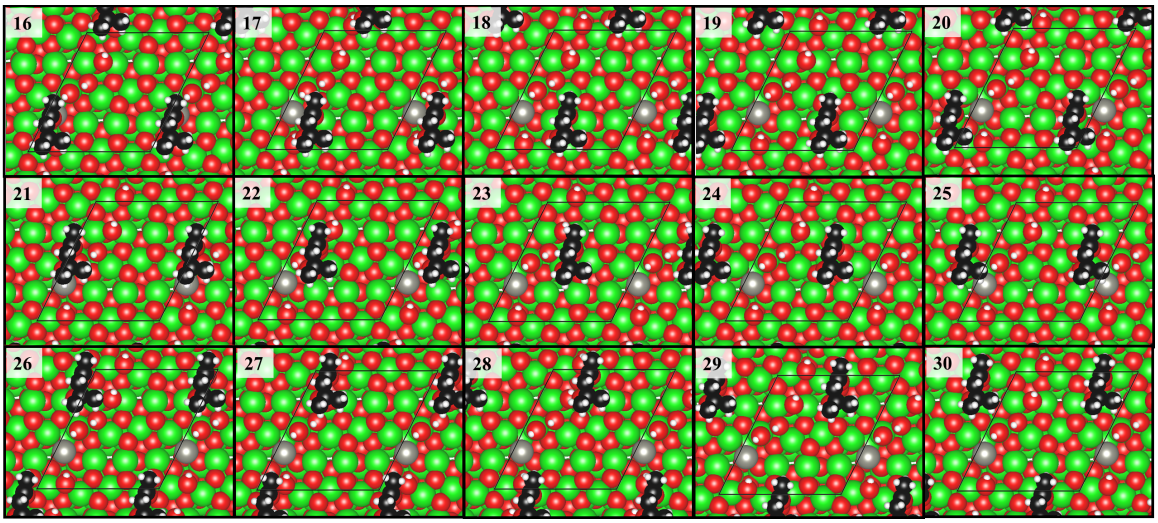

Figure S23. Top view for the vertical configuration of DAA adsorbed at plausible positions on the Hydrated Surface 2. The Zr, Zn, C, O and H atoms or ions are represented by green, gray, black, red, and white spheres, respectively.

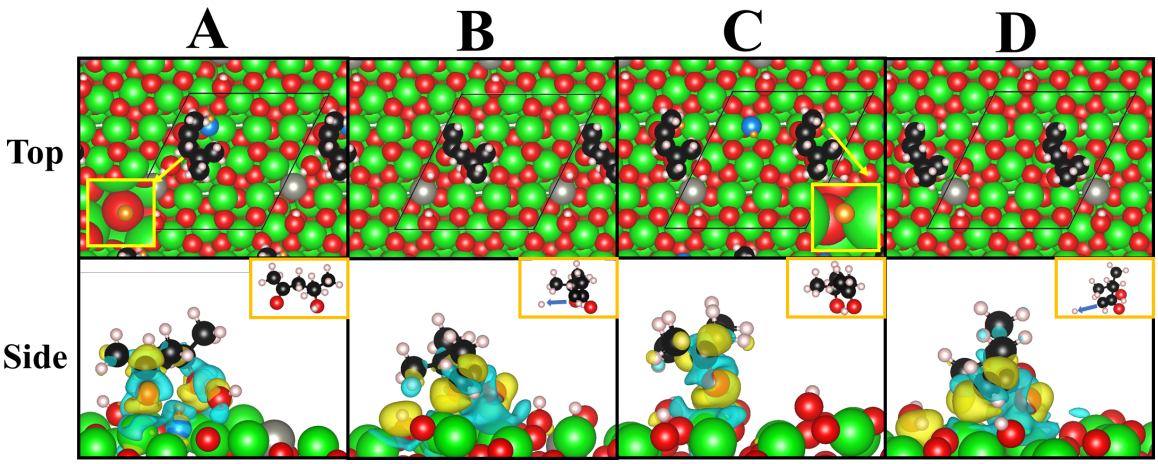

Figure S24. Top and side view of DAA at the sites within the vicinity of the adsorbed H on Hydrated Surface 2 (A, C); at the corresponding sites on the dehydrated $Zn_1Z_{11}O_{12}$ surface (B, D). The Zr, Zn, C, O and H atoms or ions are represented by green, gray, black, red, and white spheres, respectively. The surface-adsorbed O and H atoms are represented by blue and orange spheres in the top views, respectively, for clarity. The partial charge densities are presented by yellow isosurfaces for electron gains and by blue isosurfaces for electron losses with an isosurface value of 0.002 electrons/Bohr^3.

Table S1. Adsorption energy, distortion energy and number of transferred electrons for systems in Figure S23.

Site	A	B	C	D
Adsorption Energy (eV)	-2.16	-3.83	-0.91	-3.60
Distortion Energy (eV)	0.70	4.90	0.52	4.72

Transferred Electron No.	1.20	1.85	1.61	1.74

The adsorption of the DAA was compared within and outside of the surface proton vicinity in **Figure S24 A, C**, and **Figure S24 B, D**, respectively. The adsorption energies, distortion energies and number of transferred electrons in **Figure S24** are listed in **Table S1**.

When DAA outside of the surface OH vicinity, the adsorption energies are on average stronger by 2.18 eV as compared to when DAA adsorbs close to it. When DAA adsorbs far from a surface proton, a relatively high charge transfer of ~1.80 electrons indicate that a strong interaction occurs between the functional groups of DAA and the surface ions (**Figure S24 B, D**), leading to dramatic deformations with high distortion energy of ~4.81 eV. The strong interaction between the hydroxyl functional group and the surface Zr^{4+} cations results in a structural deformation of DAA, which may be responsible for the dehydration reactions where O-H bond cleavage occurs within the hydroxyl functional group of DAA (**Figure S24 B**) as well as C-H bond cleavage in the methyl functional group (**Figure S24 D**). When DAA absorbs within the vicinity of surface H, the H-atom physically hinders the FGs' interaction with the surface. As a result, the relative charge transfer decreases to ~1.40 electrons, indicating that the surface H facilitates weaker bonding between the DAA and the surface ions, leading to a low distortion energy of 0.61 eV. Thus, the surface proton plays a significant role in protecting the DAA from coking.

S2.

Derivation of the rate equation for the acetone-DAA-isobutene kinetic model

S2.1 Proposed sequence of reaction steps in acetone-DAA-isobutene over $Zn_1Zr_{10}O_z$:

(1) Acetone adsorption: $\mathrm{Ace} + * \overset{K_{\mathrm{ads,Ace}}}{\Longleftrightarrow} \mathrm{Ace}*$ **quasi-equilibrated**, $K_{\mathrm{ads,Ace}}$

(2) $\mathrm{H_2O}$ adsorption: $\mathrm{H_2O} + * \overset{K_{\mathrm{ads,H_2O}}}{\Longleftrightarrow} \mathrm{H_2O}*$ **quasi-equilibrated**, $K_{\mathrm{ads,H_2O}}$

(3) Acetone $\mathrm{C-C}$ coupling: $\mathrm{Ace}* + \mathrm{Ace} \underset{k_{C6}}{\overset{k_{-C6}}{\Longleftrightarrow}} DAA*$ **reversible**

(4) DAA $\mathrm{C-C}$ cleavage: $\mathrm{DAA}* + * \xrightarrow{k_{\mathrm{decom}}} \mathrm{CH_3COOH}* + \mathrm{IB} + *$ **irreversible, r.d.s**

(5) *A*cetic acid ketonization: $2\mathrm{CH_3COOH}* \xrightarrow{k_{\mathrm{keton}}} \mathrm{Ace}* + \mathrm{H_2O}* + \mathrm{CO_2}$ **irreversible, fast**

S2.2 Assumptions:

1. Acetone adsorption and water adsorption are quasi-equilibrated.

2. Water hinders the formation of MSO, the DAA dehydration could be ignored (MSO was barely detected in the kinetic measurements).

3. Considering the low conversion during the kinetic rate measurements (conversion<7%) and the relatively high energy of enolate, adsorbed DAA as well as water dissociation products on $Zn_1Zr_{10}O_z$, the surface coverage of enolate, DAA and OH* could be ignored compared with adsorbed water and acetone.

4. Acetone to DAA conversion is thermodynamically unfavorable at high temperatures, therefore we assume that DAA reverse reaction is much faster than its C-C cleavage ($k_{-C6}>>k_{decom}$) at the conditions we studied.

S2.3 Rate derivation and site balance:

(1)Acetone adsorption: $\mathrm{Ace} + * \overset{K_{\mathrm{ads,Ace}}}{\Longleftrightarrow} \mathrm{Ace}*$ **quasi-equilibrated**, $K_{\mathrm{ads,Ace}}$

$$[\mathrm{Ace}*] = K_{\mathrm{ads,Ace}} P_{\mathrm{Ace}} [*]$$

(2)$\mathrm{H_2O}$ adsorption: $\mathrm{H_2O} + * \overset{K_{\mathrm{ads,H_2O}}}{\Longleftrightarrow} \mathrm{H_2O}*$ **quasi-equilibrated**, $K_{\mathrm{ads,H_2O}}$

$$[\mathrm{H_2O}*] = K_{\mathrm{ads,H_2O}} P_{\mathrm{H_2O}} [*]$$

(3)Acetone $\mathrm{C-C}$ coupling: $\mathrm{Ace}* + \mathrm{Ace} \underset{k_{\mathrm{C6}}}{\overset{k_{-\mathrm{C6}}}{\Longleftrightarrow}} \mathrm{DAA}*$ **reversible**

(4)DAA $\mathrm{C-C}$ cleavage: $\mathrm{DAA}* + * \overset{k_{\mathrm{decom}}}{\longrightarrow} \mathrm{CH_3COOH}* + \mathrm{IB} + *$ **irreversible, r.d.s**

$$\frac{d[\mathrm{DAA}*]}{dt} = k_{\mathrm{C6}}[\mathrm{Ace}*]P_{\mathrm{Ace}} - k_{-\mathrm{C6}}[\mathrm{DAA}*] - k_{decom}[\mathrm{DAA}*][*] = 0$$

$$[\mathrm{DAA}*] = \frac{k_{\mathrm{C6}}[\mathrm{Ace}*]P_{\mathrm{Ace}}}{k_{-\mathrm{C6}} + k_{decom}[*]} = K_{\mathrm{DAA}} K_{\mathrm{ads,Ace}} P_{Ace}^2 [*]$$

Here, $K_{DAA} = \frac{k_{C6}}{k_{-C6}+k_{decom}[*]}$

Because the conversion of acetone to DAA is thermodynamically unfavorable at high temperatures, we assume $k_{-\mathrm{C6}}>>k_{decom}$ under the condition we studied.

So, $K_{\mathrm{DAA}} = \frac{k_{\mathrm{C6}}}{k_{-\mathrm{C6}}+k_{decom}[*]} \approx \frac{k_{\mathrm{C6}}}{k_{-\mathrm{C6}}} = K_{\mathrm{C6}}$

(5)Acetic acid ketonization: $2\mathrm{CH_3COOH}* \overset{k_{\mathrm{keton}}}{\longrightarrow} \mathrm{Ace}* + \mathrm{H_2O}* + \mathrm{CO_2}$ **irreversible, fast**

$$\frac{r_{IB}}{\mathrm{L}} = k_{\mathrm{decom}}[\mathrm{DAA}*][*] = k_{\mathrm{decom}} K_{\mathrm{C6}} K_{\mathrm{ads,Ace}} P_{\mathrm{Ace}}^2 [*]^2$$

r_{IB}, L, and [*] denote isobutene formation rate, total amount Lewis acid sites on surface and the empty active sites.

Site balance:

$$[*] = \frac{[*]}{[*] + [\mathrm{Ace}*] + [\mathrm{H_2O}*]} = \frac{1}{1 + K_{\mathrm{ads,Ace}} P_{\mathrm{Ace}} + K_{\mathrm{ads,H_2O}} P_{\mathrm{H_2O}}}$$

$$\frac{r_{IB}}{\mathrm{L}} = \frac{k_{\mathrm{decom}} K_{\mathrm{C6}} K_{\mathrm{ads,Ace}} P_{\mathrm{Ace}}^2}{(1 + K_{\mathrm{ads,Ace}} P_{\mathrm{Ace}} + K_{\mathrm{ads,H_2O}} P_{\mathrm{H_2O}})^2}$$

References:

(1) Sun, J.; Baylon, R. A. L.; Liu, C.; Mei, D.; Martin, K. J.; Venkitasubramanian, P.; Wang, Y., Key Roles of Lewis Acid–Base Pairs on $Zn_xZr_yO_z$ in Direct Ethanol/Acetone to Isobutene Conversion. *J. Am. Chem. Soc.* **2016,** *138* (2), 507-517.
(2) Herrmann, S.; Iglesia, E., Selective Conversion of Acetone to Isobutene and Acetic Acid on Aluminosilicates: Kinetic Coupling between Acid-Catalyzed and Radical-Mediated Pathways. *J. Catal.* **2018,** *360*, 66-80.
(3) Levenspiel, O., Experimental search for a simple rate equation to describe deactivating porous catalyst particles. *J. Catal.* **1972,** *25* (2), 265-272.
(4) Rorrer, J. E.; Toste, F. D.; Bell, A. T., Mechanism and Kinetics of Isobutene Formation from Ethanol and Acetone over $Zn_xZr_yO_z$. *ACS Catal.* **2019**, 10588-10604.